Special issue article

SURFACE and INTERFACE ANALYSIS

Received: 10 March 2014 Accepted: 12 March 2014 Published online in Wiley Online Library

(wileyonlinelibrary.com) DOI 10.1002/sia.5516

Atomic layer superconductivity

Agnieszka Stępniak,[a]* Augusto Leon Vanegas,[a,b] Michael Caminale,[a] Hirofumi Oka,[a] Dirk Sander[a] and Jürgen Kirschner[a,b]

We present scanning tunneling microscopy (STM) studies of superconductivity of single layer Pb and Pb islands on Si(111). We perform temperature-dependent measurements of the differential conductance from 0.38 to 4 K in fields of up to 6 T to extract the critical temperature T_C for the onset of superconductivity. We find $T_C = 1.5$ K for a single layer Pb on Si(111), and a critical out-of-plane field of 150 mT. This deviates from bulk Pb, where $T_C = 7.2$ K and $H_C = 80$ mT are reported. Our results provide the temperature dependence of the superconducting gap 2Δ. A description of this dependence in the framework of the Bardeen–Cooper–Schrieffer theory indicates an energy gap of $2\Delta_0 = 0.7$ meV, considerably less than the 2.7 meV found for bulk Pb. We observe that the insertion of a single layer Ag between Pb and Si suppresses superconductivity in the Pb film even at the lowest temperature of 0.38 K. Pb islands on Ag/Si(111) exhibit superconductivity. Our position-dependent STM studies from a nine-layer tall Pb island into the surrounding non-superconducting Pb wetting layer on Ag/Si(111) reveal an extension of a superconducting gap in spectroscopy up to 20 nm away from the Pb island edge at 0.38 K. © 2014 The Authors Surface and Interface Analysis Published by John Wiley & Sons Ltd.

Keywords: scanning tunneling microscopy and spectroscopy; superconductivity; proximity effect; silicon; lead; silver

Introduction

The study of superconductivity in systems of reduced dimensions has attracted considerable interest. Novel phenomena, such as changed critical temperature (T_C) and different critical field (H_C), are expected, when the size of the superconducting material is smaller than the characteristic length scales of superconductivity, such as the London penetration depth (λ_L) and the Ginzburg–Landau coherence length (ξ_{GL}). Studies in bulk Pb reveal typical length scales of $\lambda_L = 32$–39 nm and $\xi_{GL} = 51$–83 nm.[1] Lead attracts more attention in superconductivity studies, because bulk Pb is an elemental superconductor with a relatively high critical temperature ($T_C = 7.2$ K) and critical field of $H_C = 80$ mT. It shows a superconducting energy gap of $2\Delta_0 = 2.7$ meV. The impact of reduced dimensions on T_C and H_C is the topic of current research.

Recent studies of superconductivity in Pb films and islands[2–6] indicate that even a single atomic layer of Pb on Si(111) is superconducting with a critical temperature around 1.8 K.[2] We present data on temperature-dependent and field-dependent tunneling spectroscopy of a single layer Pb on Si(111) as a test case for the performance of our newly obtained ^{3}He-cooled scanning tunneling microscope (STM) with vector magnetic field. Our results confirm the original study performed by Zhang and co-workers.[2] We go beyond this first study of Pb monolayer superconductivity and find that the insertion of single layer Ag between Si and Pb suppresses superconductivity in Pb.

We exploit the atomic scale spatial resolution of the STM to study the spatial dependence of the spectroscopy upon a transition from a superconducting region to a normal conducting region. In particular, we investigated the transition from a superconducting Pb island to a metallic Pb/Ag wetting layer on Si(111). We identify an exponential decay with a characteristic length of order 10 nm, on which superconductivity faints into the normal-metal region.

Experimental

Figure 1 shows a photography of the ultrahigh vacuum chamber with the cryostat in the so-called bottom loader layout, where the scanning tunneling microscope is lowered toward the STM chamber for sample and tip transfer. The cryostat (Oxford) contains the ^{3}He-cooled ultrahigh vacuum STM (Omicron) and superconducting coils for a vector magnetic field [maximum vertical field: 6 T, maximum vectorial field $(H_x, H_y, H_z) = (1, 1, 2)$ T].

The STM reaches a lowest temperature of 0.32 K, and it can operate at this temperature for up to 24 h. Then, the ^{3}He gas load needs to be recondensed and pumped by a ^{4}He-cooled sorption pump of the STM–ultra-high vacuum (UHV) insert. During this process, the STM temperature increases from 0.32 to 1.8 K and then drops to 0.32 K again within a total cycle time of 2 h. A steady state temperature of 1.8 K can be maintained at the STM continuously by pumping on the ^{4}He cooling circuit. We achieve a holding time of 1 week, before 80 l of liquid ^{4}He needs to be refilled.

The STM chamber is connected to the UHV preparation chamber by a UHV gate valve. Sample and tip transfer between STM and preparation chamber are performed with a liquid He-cooled long travel horizontal manipulator. The STM chamber is equipped with evaporators, which allow deposition onto the

* *Correspondence to: Agnieszka Stępniak, Max-Planck-Institute für Mikrostrukturphysik, Weinberg 2, D-06120 Halle (Saale), Germany. E-mail: stepniak@mpi-halle.mpg.de*

a *Max-Planck-Institute für Mikrostrukturphysik, Weinberg 2, D-06120 Halle (Saale), Germany*

b *Martin Luther Universität, Institute of Physics, Halle (Saale), Germany*

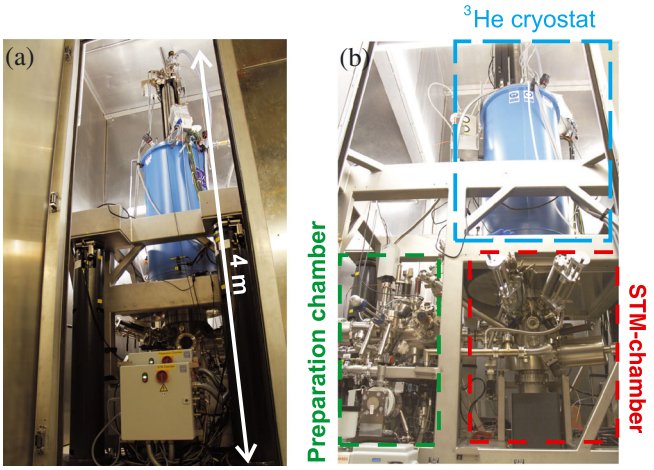

Figure 1. (a, b) Photography of the STM and preparation chamber, respectively. The setup is 4 m tall, 1.5 m wide, and 4 m long. The STM is located within a sound-proof cabin to minimize acoustic interference.

cold sample in the STM head at a temperature of order 10 K. The preparation chamber is equipped with evaporators, a differentially pumped sputter gun, tip preparation stages by e-beam heating, low-energy electron diffraction and AES experiments, and a load lock. The manipulator allows sample preparation in the range of 20–1200 K, and a high temperature stage is available for heating up to 2500 K. The Si samples used in this study are prepared by direct current heating, as indicated in Figure 2(a). The scanning tunneling microscopy/spectroscopy (STM/STS) measurements were performed in the temperature range of 0.38–4 K. The tunneling spectra were obtained by a lock-in technique with a modulation frequency of 373 Hz and a root mean square amplitude of 50 μV. We used PtIr tips for the STM, and they were prepared by cutting from a 0.25 mm wire, followed by a 5 s flash at 1700 K under UHV conditions in the preparation chamber prior to the transfer into the STM. Also electrochemically etched W-tips, which were flashed to 2300 K under UHV conditions, were used. The tunneling spectra obtained by both tips are indistinguishable. Figure 2 illustrates the preparation procedure for the multilayer Pb/Ag/Si(111) system.

An *n*-type (As: 10^{18} cm^{-3}) Si(111) single crystal (5 in. wafer, 0.62 mm thick) with a resistivity of 2–4.5 mΩ·cm was used as the substrate crystal. Rectangular specimens (12 mm × 3 mm) were cut from the Si wafer and mounted in the direct current heater sample plate, as indicated in Figure 2(a). A clean Si(111) surface was obtained by heating the sample at 1420 K under UHV conditions three times. Then, the sample was annealed at 1140 K for 15 min [Figure 2(a)] and slowly cooled down to 1070 K in 20 min. This procedure leads to the formation of a spatially extended well-ordered 7 × 7-Si(111) phase,[7] as shown in Figure 2 (b). The Ag layer was evaporated from a crucible on the 7 × 7-Si(111) surface held at 770 K within 20 min. The 7 × 7 reconstruction is lifted upon Ag deposition, and the surplus Si atoms form 3.1 Å high islands on the Si surface. Ag covers the Si islands and the Si surface in between with a regular $\sqrt{3} \times \sqrt{3}$ structure.[8,9] This is shown in Figure 2(c). Subsequently, a little more than a monolayer of Pb is first evaporated at room temperature in 20 min, followed by a post-annealing at 560 K for 1 min. This leads to the desorption of Pb in excess of the first layer,[10] and a Pb wetting layer with patches of $\sqrt{3} \times \sqrt{3}$ and $\sqrt{3} \times \sqrt{7}$ structures is

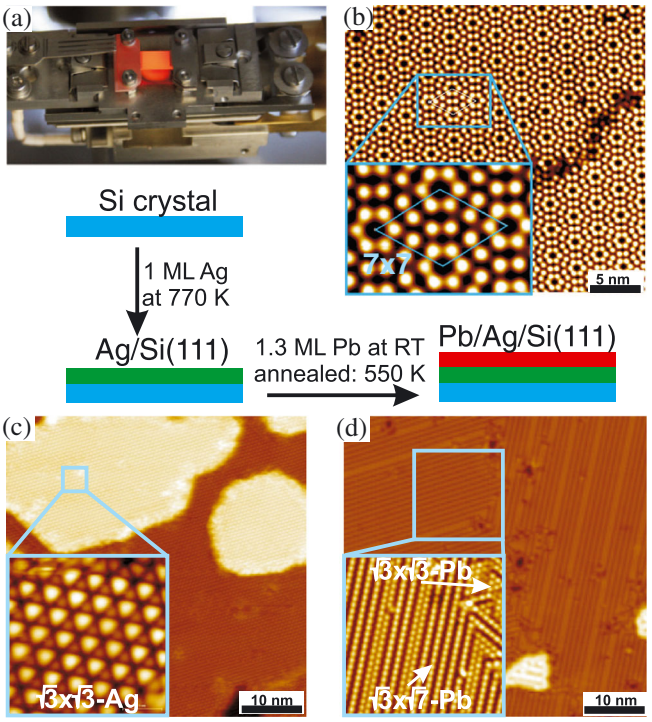

Figure 2. Preparation of the Pb/Ag/Si(111). (a) The Si crystal in the direct current heating stage in the preparation chamber during the annealing process. (b–d) Steps in the sample preparation from Si(111) to a Pb wetting layer on the Ag film on Si(111). The STM topography images present in (b) the Si(111)7 × 7 surface, (c) the $\sqrt{3} \times \sqrt{3}$-Ag coverage, and (d) the $\sqrt{3} \times \sqrt{7}$-Pb and $\sqrt{3} \times \sqrt{3}$-Pb phases. The schematics indicate the layer stacking on the Si(111) substrate.

obtained.[11] Pb islands on top of this Pb wetting layer were prepared by deposition of Pb at 240 K at a rate of 3 min/ML [1 ML: surface atomic density of Si(111): $n = 7.84$ atoms/nm^2). Pb grows in the Stranski–Krastanov mode under these conditions, and the deposition of the equivalent of 1.6 ML gives rise to the Pb island structure as shown in Figure 6.

In order to test the spectroscopy measurement capabilities of our STM, we also prepared a single layer Pb by deposition of Pb in small excess of one atomic layer onto clean 7 × 7-Si(111) surface at room temperature and annealed it at 660 K for 1–2 min. This leads to the desorption of Pb in excess of one layer.[10] Here, the Pb surface shows predominant $\sqrt{3} \times \sqrt{3}$ patches (Pb areal density: 10.44 at/nm^2) separated by $\sqrt{3} \times \sqrt{7}$ boundaries (Pb areal density: 9.40 at/nm^2), as shown in Figure 3(c). The results of this study are presented first, before we focus on spatial-dependent spectroscopy at the transition from superconducting islands to normal surroundings on the Pb/Ag/Si sample.

Results

Superconductivity of a single layer Pb on Si(111) and Ag/Si(111) surfaces

Our scanning tunneling spectroscopy (STS) study on a single layer Pb on Si(111) reveals a reduced differential conductance around the Fermi energy, which changes in a characteristic manner with temperature and field. Figures 3(a) and 4 report spectroscopy

SURFACE and INTERFACE ANALYSIS

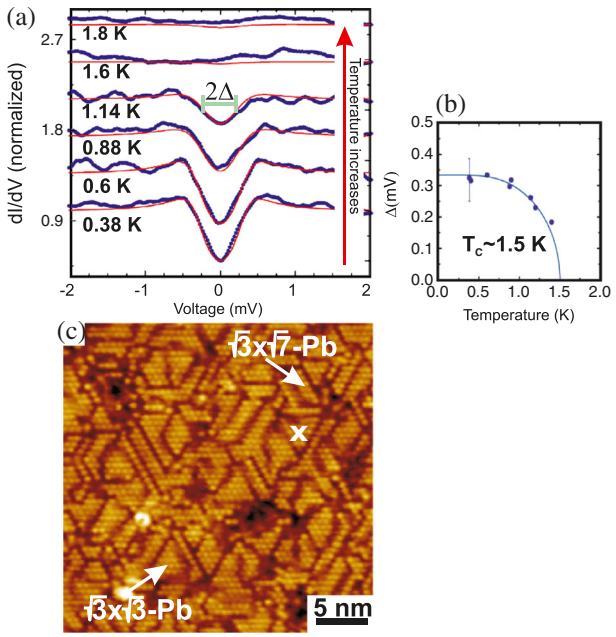

Figure 3. (a) Differential conductance spectra of a single layer Pb on Si(111). The spectra are measured on the $\sqrt{3} \times \sqrt{3}$-Pb region of the Pb wetting layer on Si(111), at the position marked by the cross on (c). The solid lines through the data points are fits with Dynes function with energy broadening $\Gamma = 0.25$ meV. This value is larger than that for thick films or island, because the energy broadening Γ is found to increase with the decreasing thickness of the superconductor and with the rising of measured temperature.[12,13] The energy gap 2Δ, as obtained by the fits through the data points, is indicated. (b) Plot of the energy gap Δ as a function of temperature. The solid line represents the temperature variation as described by the Bardeen–Cooper–Schrieffer theory. (c) Constant current STM image (30×30 nm^2) of the Pb wetting layer ($V = 5$ mV, $I = 1$ nA). Areas with $\sqrt{7} \times \sqrt{3}$ and $\sqrt{3} \times \sqrt{3}$ structures are indicated.

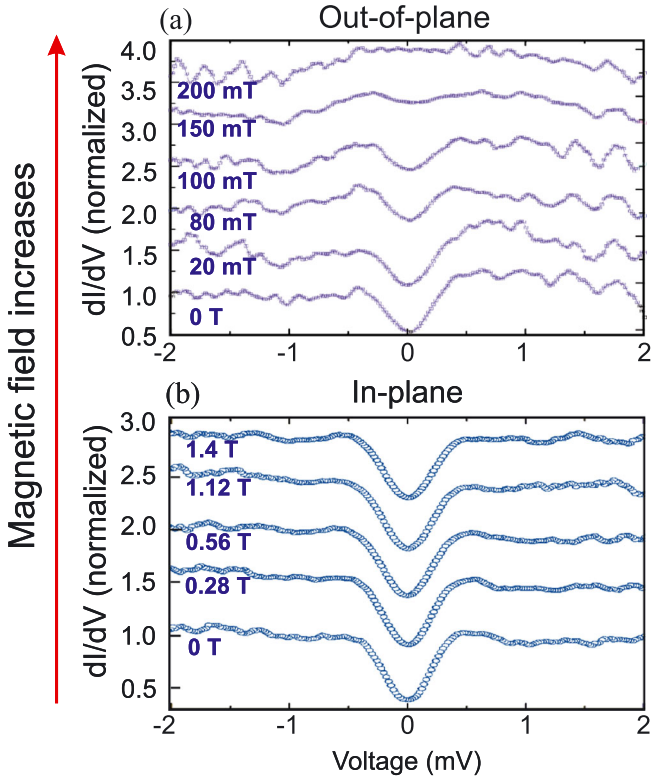

Figure 4. Superconductivity of single layer Pb on Si(111). The differential conductance dI/dV spectra as a function of magnetic field with out-of-plane (a) and in-plane (b) orientation. The tunneling junction was set at $V = 5$ mV and $I = 1$ nA.

measurements in the -2 to $+2$ mV range for both different temperatures and applied magnetic fields, respectively. All the reported spectra are normalized to the differential conductance value measured at a bias voltage of 5 mV, far from the gap region. No differences between spectra measured on the $\sqrt{3} \times \sqrt{3}$ and $\sqrt{3} \times \sqrt{7}$ phases [Figure 3(c)] could be observed.

We observe that the gap of the differential conductance becomes more shallow with increasing temperature [Figure 3(a)] and with increasing field along the out-of-plane direction [Figure 4(a)]. In particular, the gap in spectroscopy vanishes around 1.6 K at 0 T, and at an out-of-plane field of 150 mT at 0.38 K. No appreciable change of the spectra is observed for the largest in-plane field.

The dependence of the spectra on temperature and field identifies the gap feature as an indication of superconductivity of the system. This assessment is further corroborated by the successful fit of the temperature dependence of the gap width in the framework of the Bardeen–Cooper–Schrieffer theory. This treatment suggests a gap at 0 K of $\Delta(0) \approx 0.32$ meV and $T_C \approx 1.5$ K.[14] The energy gap values $\Delta(T)$ for different temperatures were extracted from a fit of the normalized dI/dV spectra employing the Dynes density of states,[15] where the parameter Γ accounts for the lifetime broadening of the quasiparticles. The field-dependent measurements of Figure 4 reveal a critical field of out-of-plane orientation of order 150 mT, whereas the critical field for in-plane orientation is larger than the maximum field of 1.4 T, which we can apply in plane.

The large critical field for the in-plane orientation, larger than 1.4 T, is in line with the expected critical field in this configuration. The critical field of a film for an in-plane field orientation is of the order $(\lambda/d)H_C$ (d : thickness of the film, and H_C : the bulk critical field).[16] This gives roughly a 100-fold increase of the critical field for an in-plane orientation, leading to 8 T, well above the highest field available here. Our measurements of the critical temperature and the critical magnetic field are in quantitative agreement with previous work.[2] Thus, we conclude that our experimental system is in good shape for the study of novel phenomena.

Our first example is the study of the influence of a Ag intermediate layer between Pb and Si on the superconductivity of the Pb layer. Figure 2(d) shows the atomic resolved constant current STM image of the Pb layer on top of the Ag/Si(111) substrate. We identify a similar structure as compared with the growth of Pb directly on Si discussed earlier. Most of the samples show the stripe phase indicative of the $\sqrt{3} \times \sqrt{7}$ structure. Relatively small areas and boundary domains show the $\sqrt{3} \times \sqrt{3}$ phase. Figure 5 presents the STS measurements on the Pb/Ag/Si(111) surface as a function of temperature and magnetic field. The STS measurements show spectral features that do not change appreciably with temperature or field, in sharp contrast to the spectra shown earlier in Figures 3 and 4(a). We conclude that the spectral feature, which at first sight could be mistaken for a gap indicative of

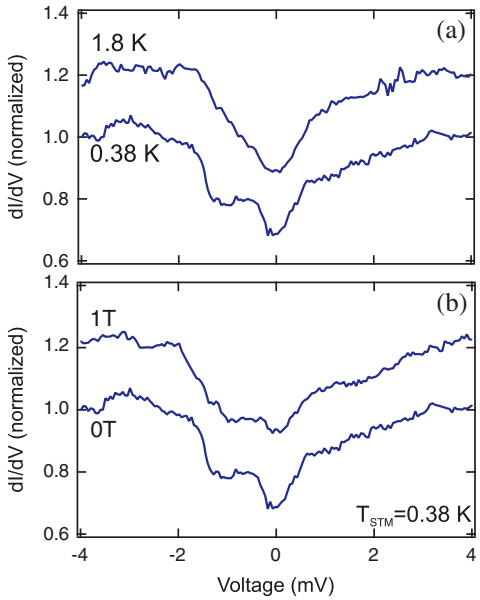

Figure 5. Differential conductance spectra of a single layer Pb on Ag/Si(111) temperature (a) and magnetic field with out-of-plane orientation (b) present a persistence of the spectral feature around 0 mV, irrespective of temperature and field. The tunneling junction was stabilized at $V = 5$ mV and $I = 1$ nA before the spectra were taken.

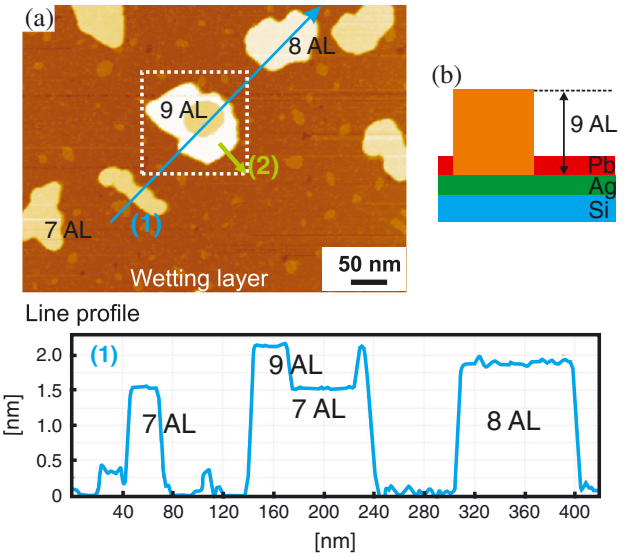

Figure 6. (a) STM topography image of Pb islands on the Pb wetting layer on Ag/Si(111). The size of the image is 530 × 400 nm. The solid blue line indicates the line profile (1), shown in the lower panel. The green arrow (2) indicates the direction of the line scan along which the spatial dependence of spectroscopy is measured, as shown in Figure 7(b). (b) Sketch of the layer stacking of the sample at the island position. Heights of the islands were determined from the peak positions of the quantum well states.

superconductivity, is solely a characteristic of the electronic structure of the Pb/Ag/Si system. Thus, the insertion of a Ag layer in between Pb and Si inhibits superconductivity in the Pb layer.

We speculate that the modified bonding situation at the interface is responsible for the loss of superconductivity. The insertion of Ag inhibits a direct covalent bond between Pb and Si, and this is expected to be a main aspect of superconductivity in the Pb layer, according to theoretical work.[17] Next, we illustrate how superconductivity spills out from a Pb island into the surrounding non-superconducting Pb/Ag/Si(111) surface.

Superconductivity and proximity effect of Pb islands grown on the Pb/Ag/Si(111) surface

In Figure 6, we present a topography overview of the sample with Pb islands grown on Pb/Ag/Si(111). The non-superconducting substrate was prepared as described earlier (see also Figure 2), and then, additional Pb was deposited at 240 K, forming islands on the wetting layer.

A line scan through the islands along the blue line of Figure 6(a) reveals three different island heights. Figure 6(b) shows the sketch of the layer stacking of the sample. The constant current line profile gives only information about the apparent heights of the system, because of the different structural and electronic properties of island and wetting layer. We determine the island height from the quantitative analysis of spatial resolved electron spectroscopy, which identifies quantum well states (QWS). The energy dependence of QWS allows a thickness calibration along the vertical direction.[18]

Pb growth under these conditions follows the Stranski–Krastanov scenario. Pb islands with atomically flat (111) oriented surfaces form, where atomic-layer depressions in the island top are observed. The island edges are mostly aligned along the equivalent Si $< 1\bar{1}0 >$ crystallographic directions.[19,20] To obtain atomically flat top island surfaces without depressions, the sample needs to be annealed at 300 K after the deposition,[20,21] causing, however, a significant increase of the lateral island dimensions. We do not anneal the sample at 300 K, and we obtain islands with void structures or small clusters on top. But we benefit from a better control of island height and lateral size.

We observed three characteristic heights of islands: 7, 8, and 9 AL. Here, 1 AL corresponds to the (111) single atomic plane of Pb, with a height of 0.286 nm. This finding is in agreement with the formerly proposed argument that QWS favor the formation of islands with distinct heights.[19]

As a consequence of the islands' growth, the Pb single layer surface, the so-called wetting layer, also changes its morphology. Apart from $\sqrt{3}\times\sqrt{3}$ and $\sqrt{3}\times\sqrt{7}$ structures, a significant number of clusters and atoms of Pb is also observed.

To study the spatial variation of spectroscopy upon a transition from the superconducting island toward the surrounding wetting layer, we focus on the 9 AL height and 100 nm wide island within the white dashed square shown in Figure 6. The differential conductance spectra measured at the edge of the island reported in Figure 7(d) clearly show a superconducting gap, which is about 2 mV wide at 0.38 K. The critical temperature and critical magnetic field along the out-of-plane direction were found to be above 5 K and 0.8 T, respectively.

We performed measurements of the differential conductance with sub-nanometer spatial resolution away from the island, along the direction of the green arrow, as depicted in Figure 6. The resulting spectra measured at 0.38 K are stacked in the 2D plot shown in Figure 7(b). Here, the *x*-axis is the distance, the *y*-axis is the applied bias voltage, and the color code represents the differential conductance value. The dark, brown, and white colors indicate low, normal, and enhanced differential

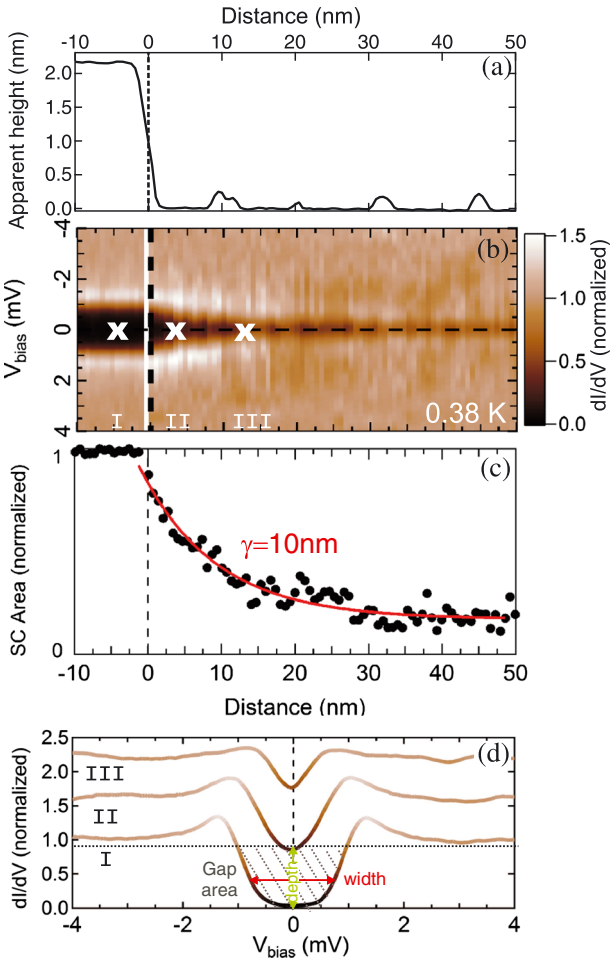

Figure 7. (a) Constant current line profile along the 9 AL Pb island into the wetting layer, as indicated by the green line (2) in the Figure 6(a). (b) Spatial dependence of the differential conductance spectra, measured along the line of (a) at 0.38 K. Panel (c) shows the normalized gap area as a function of distance from the island edge, as extracted from the spectra contained in (b). The solid red line is an exponential fit. (d) Local tunneling conductance spectra acquired on the island (I), on the wetting layer 4 nm away from the island edge (II) and 15 nm away from the island (III). The spectra are normalized to unity and shifted vertically for clarity. The gap area is hashed to illustrate its definition.

conductance, respectively. Thus, the dark region around 0 mV indicates superconductivity. Three spectra extracted from the 2D stacking are shown in Figure 7(d) for clarity. The plot in Figure 7(b) indicates that the gap (identified by the dark area) is constant up to the island edge and it fades gradually moving away from the edge.

We aim for a quantitative characterization of the decay length of the spectroscopy gap. Thus, we extract the area of the spectroscopic gap feature, illustrated in Figure 7(d), as an indicator of the superconducting state of the surface. Previously, the zero bias conductance has been established to characterize superconductivity.[22] This values remains zero well below T_C, and it is thus insensitive to the subtle changes of the gap feature. We propose that the gap area better represents superconductivity, as it is sensitive to both gap depth and width. We extract this value from each differential conductance spectrum collected in Figure 7(b) and plot it as a function of distance in Figure 7(c). The area is normalized to the gap area of the first spectrum on the island.

In order to quantify the decay length for the induced superconductivity in our system, we fit the spatial dependence of the gap area with an exponential function ($e^{-x/\gamma}$). The exponential function nicely reproduces the experimental result, as indicated by the solid red line through the data points. This fit provides a decay length γ of about 10 nm at 0.38 K.

Given that the induced superconductivity is caused by the proximity of the superconducting Pb island, we can compare the resulting decay length γ with the coherence length ξ, which characterizes superconductivity in the island. In the framework of the Ginzburg–Landau theory, we exploit the relation between the coherence length ξ and the critical field $H_C = \Phi_0/(2\pi\xi^2)$, where Φ_0 is the magnetic flux quantum.[16] Our measured critical field of the island is $H_C = 0.8$ T, and we obtain a coherence length ξ of 20 nm, in qualitative agreement with the length scale on which superconductivity decays into the wetting layer, as shown in Figure 7.

However, we suspect that in addition to the coherence length of the Pb islands, also, the characteristics of the wetting layer should influence the length scale of the induced superconductivity. Important aspects in this respect are the structure of the junction between the wetting layer and the island, the wetting layer morphology, and its electron mean free path. More work in experiment and theory is called for to arrive at a description of the relevant principles at the electronic level.

Conclusion and outlook

Using scanning tunneling microscopy and spectroscopy, we studied superconductivity of a single layer Pb on Si(111) and Ag/Si(111). We observed superconductivity in one-layer Pb film on Si(111), with a critical temperature of 1.5 K. The critical field H_C for the layer is of order of 150 mT. We find that an interlayer of Ag suppresses superconductivity in single layer Pb. This new finding sheds fresh light onto the electronic origins of superconductivity in single layer Pb on Si. It points at the importance of the covalent bond between Pb and Si to obtain superconductivity. Studies of the spatial extension of superconductivity revealed at length scale of order 10 nm at which superconductivity decays into the wetting layer. Future experiments will explore superconductivity on the nanometer scale in the presence of competing spin-ordering mechanisms.

References

[1] W. Buckel, R. Kleiner, *Supraleitung*, Wiley, Weinheim, **2004**.
[2] T. Zhang, P. Cheng, W.-J. Li, Y.-J. Sun, G. Wang, X.-G. Zhu, K. He, L. Wang, X. Ma, X. Chen, Y. Wang, Y. Liu, H.-Q. Lin, J.-F. Jia, Q.-K. Xue, *Nature Phys.* **2010**, *6*, 104.
[3] T. Nishio, M. Ono, T. Eguchi, H. Sakata, Y. Hasegawa, *Appl. Phys. Lett.* **2006**, *88*, 113115.
[4] C. Brun, I. P. Hong, F. Patthey, I. Y. Sklyadneva, R. Heid, P. M. Echenique, K. P. Bohnen, E. V. Chulkov, W. D. Schneider, *Phys. Rev. Lett.* **2009**, *102*, 207002.
[5] S. Qin, J. Kim, Q. Niu, C. K. Shih, *Science* **2009**, *324*, 1314.
[6] T. Cren, D. Fokin, F. Debontridder, V. Dubost, D. Roditchev, *Phys. Rev. Lett.* **2009**, *102*, 127005.
[7] B. S. Schwartzentruber, Y.-W. Mo, M. B. Webb, M. G. Legally, *J. Vac. Sci. Technol. A* **1989**, *7*, 2901.

[8] N. Sato, T. Nagao, S. Hasegawa, *Surf. Sci.* **1999**, *442*, 65.
[9] H. Aizawa, M. Tsukada, N. Sato, S. Hasegawa, *Surf. Sci.* **1999**, *429*, L509.
[10] E. Ganz, I.-S. Hwang, F. Xiong, S. K. Theiss, J. Golovchenko, *Surf. Sci.* **1991**, *257*, 259.
[11] K. Horikoshi, X. Tong, T. Nagao, S. Hasegawa, *Phys. Rev. B* **1999**, *60*, 13287.
[12] S. Bose, A. M. García-García, M. M. Ugeda, J. D. Urbina, C. H. Michaelis, I. Brihuega, K. Kern, *Nat. Mater.* **2010**, *9*, 550.
[13] J. Liu, X. Wu, F. Ming, X. Zhang, K. Wang, B. Wang, X. Xiao, *J. Phys.: Condens. Matter.* **2011**, *23*, 265007.
[14] J. Bardeen, L. N. Cooper, I. R. Schrieffer, *Phys. Rev.* **1957**, *108*, 1175.
[15] R. C. Dynes, V. Narayanamurti, J. P. Garno, *Phys. Rev. Lett.* **1978**, *41*, 1509.
[16] M. Tinkham, *Introduction to Superconductivity*, McGraw-Hill, New York, **1996**.
[17] J. Noffsinger, M. L. Cohen, *Solid States Comunications* **2011**, *151*, 421.
[18] M. C. Yang, C. L. Lin, W. B. Su, S. M. Lu, H. Y. Lin, C. S. Chang, W. K. Hsu, T. T. Tsong, *Phys. Rev. Lett.* **2009**, *102*, 196102.
[19] M. Hupalo, M. C. Tringides, *Phys. Rev. B* **2007**, *75*, 235443.
[20] F. Palmino, Ph. Dumas, Ph. Mathiez, C. Mouttet, F. Salvan, *Ultramicroscopy* **1992**, *42-44*, 928–932.
[21] M. Hupalo, V. Yeh, L. Berbil-Bautista, S. Kremmer, E. Abram, M. C. Tringides, *Phys. Rev. B* **2001**, *64*, 155307.
[22] J. Kim, V. Chua, G. A. Fiete, H. Nam, A. H. McDonald, Ch.-K. Shih, *Nature Phys.* **2012**, *8*, 464.